Supplement of Earth Surf. Dynam., 10, 909–928, 2022
https://doi.org/10.5194/esurf-10-909-2022-supplement

Earth Surface Dynamics
Open Access
EGU

Supplement of

Quantification of post-glacier bedrock surface erosion in the European Alps using ^{10}Be and optically stimulated luminescence exposure dating

Joanne Elkadi et al.

Correspondence to: Joanne Elkadi (joanne.elkadi@unil.ch)

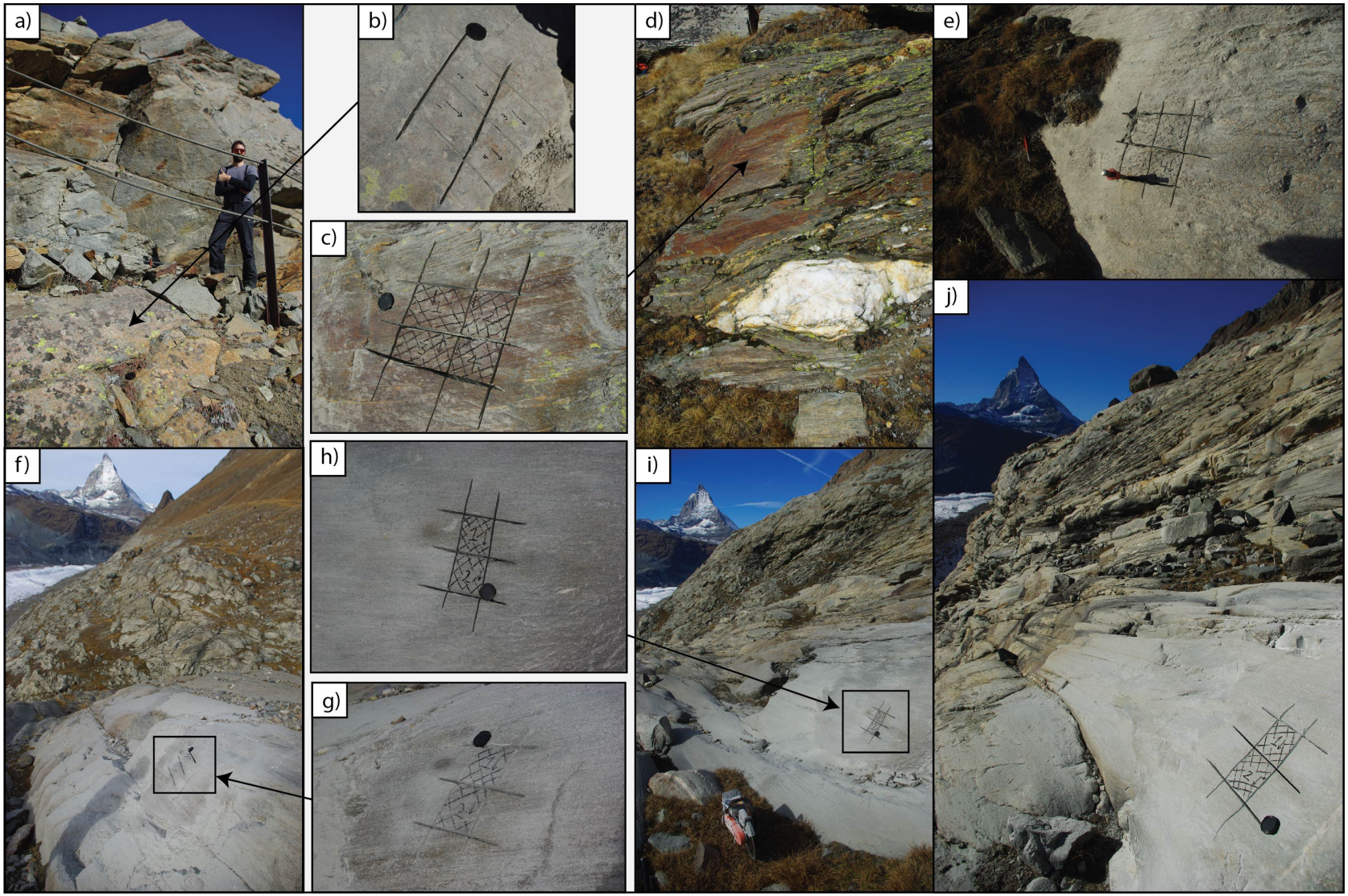

Figure S1: Images of sampling sites and surface morphologies for samples GG01 (a-b), GG02 (c-d), GG03 (e), GG04 (f-g), GG05 (h-i) and GG06 (j).

Table S1: Summary of inverted OSL parameters and bleaching depths of the two calibration samples for Sample GG05. The South facing sample has the same orientation as the unknown age sample, and the East facing sample is in a different orientation. The inflection point of the luminescence profiles (luminescence signal = 0.5) is used as a proxy for the bleaching depth.

Orientation	μ (mm^{-1})	+1 σ	-1 σ	+2 σ	-2 σ	$\overline{\sigma\varphi_0}$ (s^{-1})	+1 σ	-1 σ	+2 σ	-2 σ	Bleaching depth (mm)
$IRSL_{50}$											
South	1.55	1.85	1.25	2.05	1.05	1.14 x 10^{-6}	2.84 x 10^{-6}	4.54 x 10^{-7}	4.49 x 10^{-6}	2.87 x 10^{-7}	2.55
East	1.45	1.65	1.15	1.95	1.05	4.48 x 10^{-7}	8.94 x 10^{-7}	2.25 x 10^{-7}	1.42 x 10^{-6}	1.42 x 10^{-7}	2.09
OSL_{125}											
South	1.55	2.05	1.25	2.35	1.05	4.48 x 10^{-7}	1.12 x 10^{-6}	2.45 x 10^{-7}	2.24 x 10^{-6}	1.13 x 10^{-7}	1.95
East	1.55	1.95	1.25	2.25	1.05	1.78 x 10^{-7}	3.56 x 10^{-7}	1.42 x 10^{-7}	5.64 x 10^{-7}	1.13 x 10^{-7}	1.35
post-IR $IRSL_{225}$											
South	2.05	2.65	1.65	2.85	1.25	3.51 x 10^{-7}	8.72 x 10^{-7}	1.77 x 10^{-7}	1.12 x 10^{-7}	1.37 x 10^{-6}	1.36
East	1.95	2.55	1.45	2.75	1.25	1.55 x 10^{-7}	2.62 x 10^{-7}	1.09 x 10^{-7}	3.72 x 10^{-7}	1.09 x 10^{-7}	1.01

Table S2: Summary of inverted $IRSL_{50}$ unknown parameters for all sample sites. The values presented are the median, calculated from the retained values following the rejection algorithm outlined in Section 2.2.

Site ID	$\dot{D}$ (Gy ka^{-1})	μ (mm^{-1})	+1σ	-1σ	$\overline{\sigma\varphi_0}$ (s^{-1})	+1σ	-1σ	t (a)	+1σ	-1σ
GG01	5.1	1.5	1.6	1.2	9.2E^{-7}	1.8E^{-6}	4.8E^{-7}	24.4	16.0	32.7
GG02	6.8	0.6	0.7	0.6	1.4E^{-7}	1.6E^{-7}	1.2E^{-7}	15.2	11.1	19.3
GG03	4.9	1.6	1.8	1.3	1.1E^{-6}	2.8E^{-6}	5.7E^{-7}	107.6	59.0	166.0
GG04	4.9	2.5	2.8	2.2	1.4E^{-6}	2.3E^{-6}	7.1E^{-7}	96.4	47.0	165.5
GG05	6.4	1.5	1.8	1.2	1.1E^{-6}	2.8E^{-6}	5.7E^{-7}	2.2	2.2	4.7
GG06	7.3	1.5	1.8	1.3	1.8E^{-6}	3.1E^{-6}	1.1^{-6}	13.5	9.3	17.7

Table S3: Summary of inverted OSL_{125} unknown parameters for all sample sites. The values presented are the median, calculated from the retained values following the rejection algorithm outlined in Section 2.2.

Site ID	$\dot{D}$ (Gy ka^{-1})	μ (mm^{-1})	$+1\sigma$	-1σ	$\overline{\sigma\varphi_0}$ (s^{-1})	$+1\sigma$	-1σ	t (a)	$+1\sigma$	-1σ
GG01	5.1	1.8	2.1	1.6	2.6E^{-7}	3.7E^{-7}	1.8E^{-7}	17.9	8.1	37.6
GG02	6.8	1.5	1.8	1.2	2.2E^{-7}	5.6E^{-7}	1.1E^{-7}	65.7	15.9	145.3
GG03	4.9	1.3	1.8	1.0	1.5E^{-6}	4.6E^{-6}	6.2E^{-7}	6.0	6.0	25.9
GG04	4.9	2.6	2.9	2.2	1.8E^{-7}	2.8E^{-7}	1.1E^{-7}	65.7	25.9	135.3
GG05	6.4	1.8	2.5	1.3	2.8E^{-7}	7.1E^{-7}	1.4E^{-7}	6.0	6.0	15.9
GG06	7.3	1.2	1.4	1.1	1.3E^{-7}	1.6E^{-7}	1.1E^{-7}	5.6	5.6	5.6

Table S4: Summary of inverted post-IR $IRSL_{225}$ unknown parameters for all sample sites. The values presented are the median, calculated from the retained values following the rejection algorithm outlined in Section 2.2.

Site ID	$\dot{D}$ (Gy ka^{-1})	μ (mm^{-1})	$+1\sigma$	-1σ	$\overline{\sigma\varphi_0}$ (s^{-1})	$+1\sigma$	-1σ	t (a)	$+1\sigma$	-1σ
GG01	5.1	1.5	1.8	1.4	1.7E^{-7}	2.2E^{-7}	1.2E^{-7}	7.1	7.1	17.0
GG02	6.8	1.1	1.3	1.0	1.1E^{-7}	1.4E^{-7}	1.1E^{-7}	117.0	68.2	175.6
GG03	4.9	1.0	1.1	1.0	7.3E^{-6}	8.8E^{-6}	6.1E^{-7}	2.0	1.7	2.7
GG04	4.9	2.7	3.9	2.4	1.4E^{-7}	2.8^{-7}	1.1E^{-7}	45.8	15.9	95.5
GG05	6.4	2.4	2.9	1.9	2.8E^{-7}	7.1E^{-7}	1.4E^{-7}	6.0	6.0	15.9
GG06	7.3	1.5	1.9	1.3	3.6E^{-7}	7.1E^{-7}	2.3E^{-7}	6.2	6.2	6.2

Influence of calibration sample orientation

For sample site 5, two calibration samples were collected in different orientations- one in the same orientation as the unknown age sample (South facing) and another facing East. The south facing calibration sample was always bleached to a deeper depth, with a difference in bleaching depth of 0.5 mm for the $IRSL_{50}$ profiles, 0.6 mm for OSL_{125} and 0.4 mm for post-IR $IRSL_{225}$. The inflection point of the luminescence profiles (luminescence signal = 0.5) was used as a proxy for the bleaching depth. This difference in the depth of signal resetting is most likely due to the southern facing samples spending a greater proportion of the day exposed to sunlight. Nevertheless, $\overline{\sigma\varphi_0}$ and μ values were calculated for both calibration samples and the results are presented in Table S1. Across the three stimulation signals, the $\overline{\sigma\varphi_0}$ and μ values all overlap within 2σ, and all within 1σ aside from for the OSL_{125} signal. This suggests that the effects of sampling a calibration sample in a different orientation to the unknown age sample are minimal.

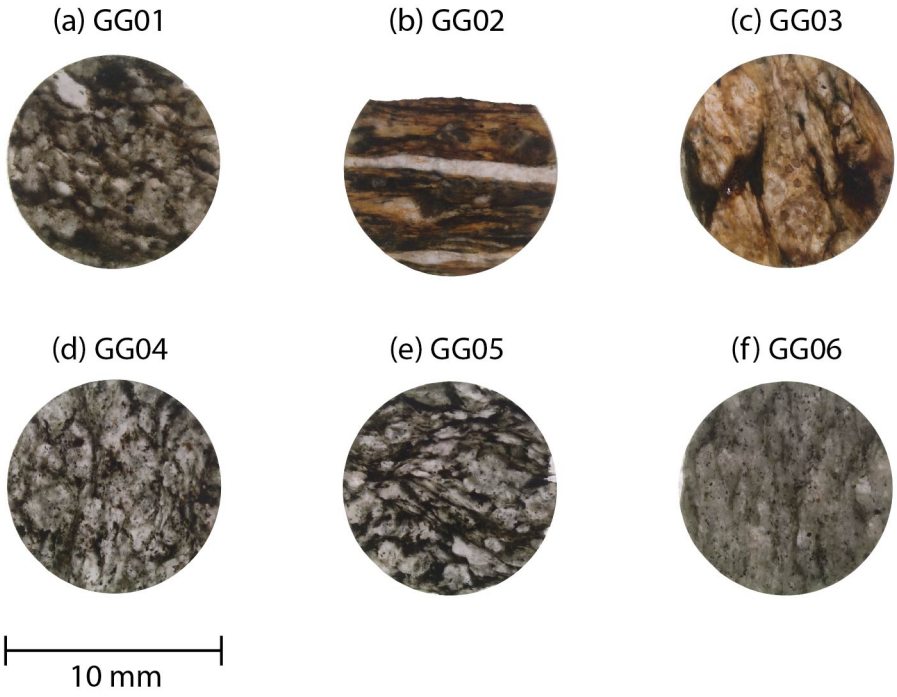

Figure S2: Images of example rock slices (10 mm diameter) for all samples in this study. Prior to the luminescence measurements, slices like this were broken into smaller fragments and placed into stainless steel cups. Sample GG01 is a hornfels, samples GG02 and GG05 are schist and samples GG03, GG04 and GG06 are gneiss. GG02 and GG03 were identified as the oldest using ^{10}Be, supported here by their red, iron-oxide tinge which is as a result of their extensive exposure to weathering.

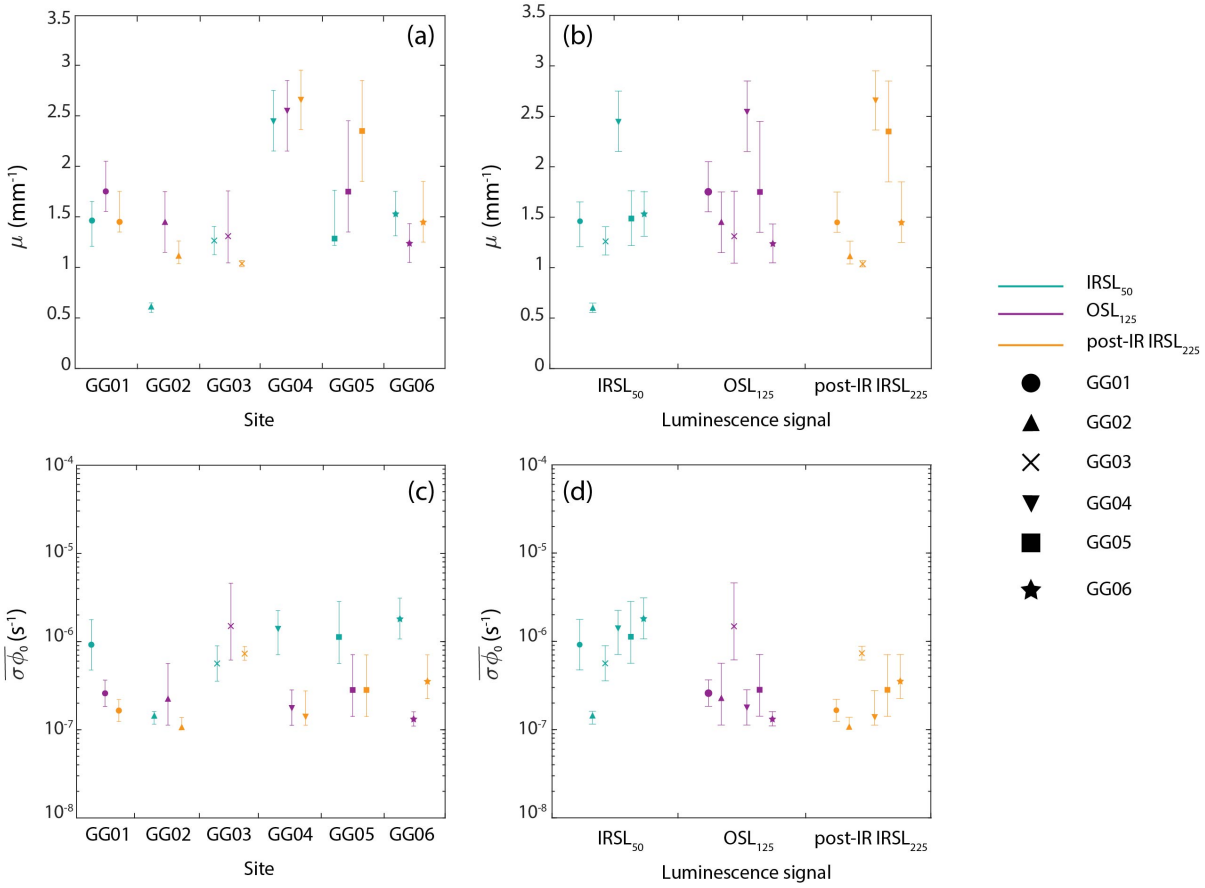

Figure S3: A comparison of the $\overline{\sigma\varphi_0}$ and μ results obtained for the three luminescence signals measured in this study- $IRSL_{50}$ (blue), OSL_{125} (purple) and post-IR $IRSL_{225}$ (orange)- by applying an inversion method on the six samples individually. The exact values can be found below in Tables S2, S3 and S4.

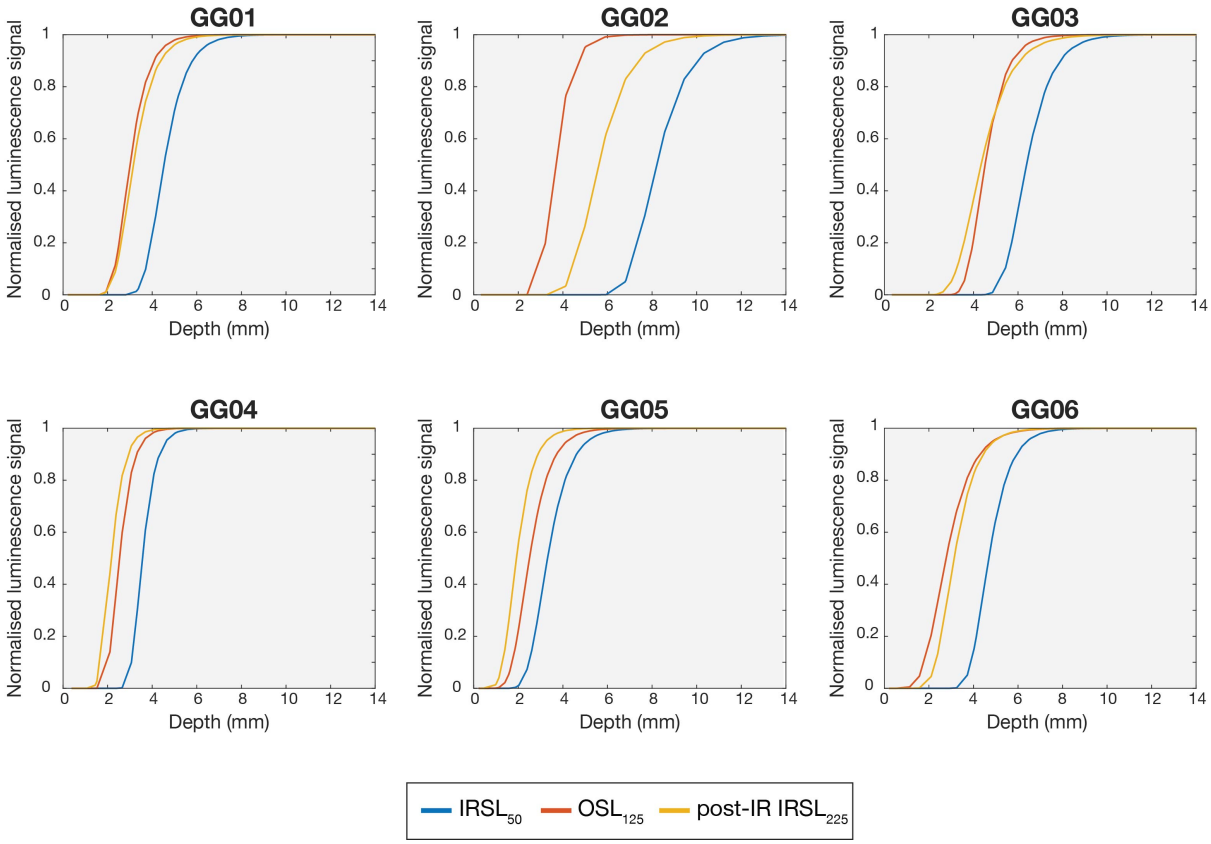

Figure S4: Model results for normalised depth profiles indicating the bleaching depths of the three luminescence signals for each sample. Note that all cores were combined prior to generating these model fits. The μ and $\overline{\sigma\varphi_0}$ values used in each plot are the median values are found in Tables S2, S3 and S4.

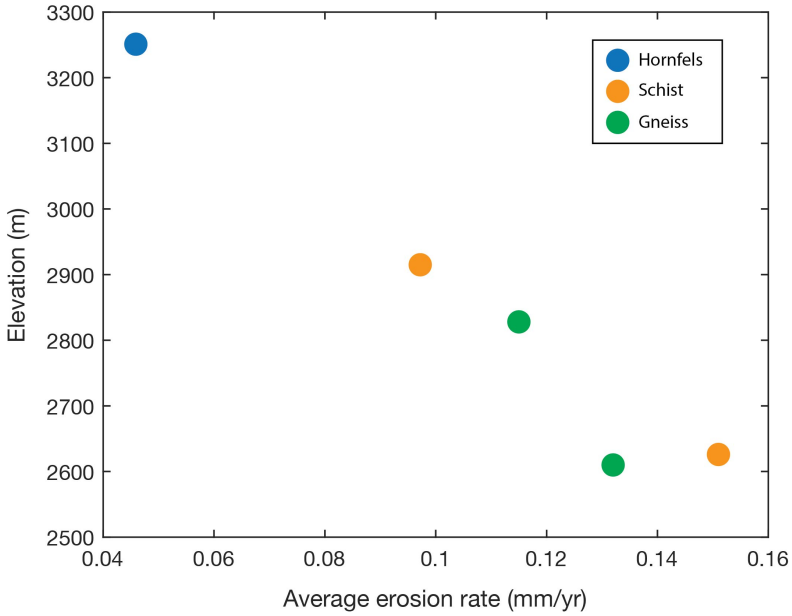

Figure S5: Distribution of inverted bedrock surface erosion rates with elevation, and colour coded according to the sample lithologies.

Influence of rainfall/precipitation with elevation

The Clausius-Clapeyron (CC) relationship states that for every 1°C rise in temperature, there is a ≈7% increase in the moisture holding capacity of the atmosphere.

Sample ID	Elevation (m)	Expected air temperature (°C)*	ΔT between highest and lowest elevation samples	% increase in moisture holding capacity of atmosphere using CC
		Gorner		
GG01	3251	-4.67	-3.52	24.67
GG02	2915	-2.82		
GG03	2828	-2.34		
GG04	2659	-1.41		
GG05	2626	-1.23		
GG06	2610	-1.15		
		Mont Blanc Massif		
MBTP1	2545	-1.00	-2.48	17.36
MBTP2	2460	-0.54		
MBAM1	2447	-0.47		
MBAM2	2363	-0.00		
MBTP11	2310	0.29		
MBAM3	2259	0.57		
MBTP5	2220	0.78		
MBTP9	2133	1.26		
MBTP6	2094	1.48		

*Air temperature estimated using a lapse rate of 5.5 °C/km, and (1) Gorner: average value from Zermatt (4.2°C at 1638 m) Meteo Suisse weather station and (2) Mont Blanc Massif: average value from Chamonix (7.3°C at 1035 m elevation) Meteo France weather station.